

Electrostatic funneling of substrate in mitochondrial inner membrane carriers

Yi Wang and Emad Tajkhorshid*

Center for Biophysics and Computational Biology, Beckman Institute for Advanced Science and Technology, and Department of Biochemistry, University of Illinois at Urbana-Champaign, Urbana, IL 61801

Edited by Barry H. Honig, Columbia University, New York, NY, and approved April 17, 2008 (received for review February 25, 2008)

Exchange of ATP and ADP across mitochondrial membrane replenishes the cytoplasm with newly synthesized ATP and provides the mitochondria with the substrate ADP for oxidative phosphorylation. The sole means of this exchange is the mitochondrial ADP/ATP carrier (AAC), a membrane protein that is suggested to cycle between two conformationally distinct states, cytosolic-open (c-state) and matrix-open (m-state), thereby shuttling nucleotides across the inner mitochondrial membrane. However, the c-state is the only structurally resolved state, and the binding site of ADP remains elusive. Here, we present $\approx 0.3 \mu\text{s}$ of all-atom MD simulations of the c-state revealing rapid, spontaneous binding of ADP to deeply positioned binding sites within the AAC lumen. To our knowledge, a complete ligand-binding event has heretofore not been described in full atomic detail in unbiased simulations. The identified ADP-bound state and additional simulations shed light on key structural elements and the initial steps involved in conversion to the m-state. Electrostatic analysis of trajectories reveals the presence of an unusually strong positive electrostatic potential in the lumen of AAC that appears to be the main driving force for the observed spontaneous binding of ADP. We provide evidence that the positive electrostatic potential is likely a common attribute among the entire family of mitochondrial carriers. In addition to playing a key role in substrate recruitment and translocation, the electropositivity of mitochondrial carriers might also be critical for their binding to the negatively charged environment of the inner mitochondrial membrane.

ADP/ATP carrier | ligand binding | mitochondrial carrier family | molecular dynamics | nucleotide translocation

In eukaryotic cells, adenosine triphosphate (ATP) is produced in the mitochondria from adenosine diphosphate (ADP) and inorganic phosphate and then exported to the cytosol, where its hydrolysis provides energy for a wide variety of cellular processes. Meanwhile, cytosolic ADP is recycled back into the mitochondria for ATP regeneration. The exchange of ADP/ATP across the inner mitochondrial membrane is achieved by a specialized membrane protein named ADP/ATP carrier (AAC) (1–9). AAC belongs to the mitochondrial carrier family (MCF), which is characterized by a tripartite structure with three homologous repeats of ≈ 100 aa, each containing a sequence motif named the MCF motif PX(D/E)XX(K/R) (10, 11). Additionally, AAC has a signature sequence, RRRMMM, which is absent in other MCF members (12).

In the inner mitochondrial membrane, AAC forms six transmembrane helices with both the amino and carboxyl termini in the intermembrane space (IMS) of mitochondria (13, 14). During an exchange cycle, AAC is suggested to undergo large conformational transitions between a cytosolic-open state (c-state), to which ADP binds from the cytoplasm, and a matrix-open state (m-state), where ATP needs to bind from the mitochondrial matrix (4, 6). Specific substrate binding to one state triggers the transition of AAC to the other state. Two families of inhibitors, atractyloside (ATR) and bongkrekic acid (BA) can abolish the activity of the protein and lock it in one of the two states: ATR stabilizes the carrier in the c-state, whereas

BA locks it in the m-state. The structure of AAC locked in the c-state by the inhibitor carboxyatractyloside (CATR) has been solved recently at 2.2 Å resolution (8). The six transmembrane helices of AAC (H1–H6) form a basin with a cone-shaped deep depression accessible from the cytosolic side (8). In each odd-numbered helix, the proline of the MCF motif introduces a sharp kink, which is suggested to act as a hinge in straightening the helices when AAC transforms to the m-state (8).

Molecular dynamics (MD) simulations have been used successfully in studying the mechanism of various membrane proteins (15–21). Here, we present MD simulations performed on an AAC monomer embedded in a lipid membrane, investigating the process of ADP binding and initial conformational changes of AAC during ADP translocation. Our results, obtained from $\approx 0.3 \mu\text{s}$ of simulations, reveal a rapid, spontaneous binding of the nucleotide, during which a strong electrostatic potential of AAC is found to play a key role. Potential binding pockets of ADP are uncovered by these simulations. To probe conformational changes of AAC during nucleotide translocation, we have also performed simulations in which an ADP molecule is biased to translocate across the carrier. These simulations suggest that outward motion of the odd-numbered helices constitutes a key structural change accompanying the ADP translocation. Finally, we will show that the identified, unusually strong electrostatic features of AAC are shared by the MCF family, which may play important roles not only in substrate binding and translocation but also in anchoring the carriers to the negatively charged environment of the inner mitochondrial membrane.

Results and Discussion

Spontaneous Binding of ADP. Four independent nucleotide binding simulations [NB1–NB4, supporting information (SI) Table S1] were performed to probe the process of ADP binding. In each simulation, an ADP molecule is initially placed on the cytosolic side of AAC, ≈ 25 Å above the bottom of the AAC vestibule (Fig. 1). To demonstrate insensitivity of the results to initial configuration, two opposite initial orientations of ADP were used: In NB1, the phosphate groups of ADP are pointed toward AAC (Fig. 1*b*), whereas in the other three binding simulations, the phosphate groups are pointed away from the protein (Fig. 1*c*). ADP molecules are found to diffuse spontaneously toward the bottom of the AAC lumen over a distance of >20 Å, penetrating deeply into the basin within only a few nanoseconds. Despite opposite initial orientations, all AAC-bound ADP molecules converge into similar final orientations, in which phosphate groups are pointing down and inserted into the binding site (Fig. 2). The only exception is simulation NB3, in which ADP was attracted by two basic residues

Author contributions: Y.W. and E.T. designed research; Y.W. performed research; Y.W. and E.T. analyzed data; and Y.W. and E.T. wrote the paper.

The authors declare no conflict of interest.

This article is a PNAS Direct Submission.

*To whom correspondence should be addressed. E-mail: emad@life.uiuc.edu.

This article contains supporting information online at www.pnas.org/cgi/content/full/0801786105/DCSupplemental.

© 2008 by The National Academy of Sciences of the USA

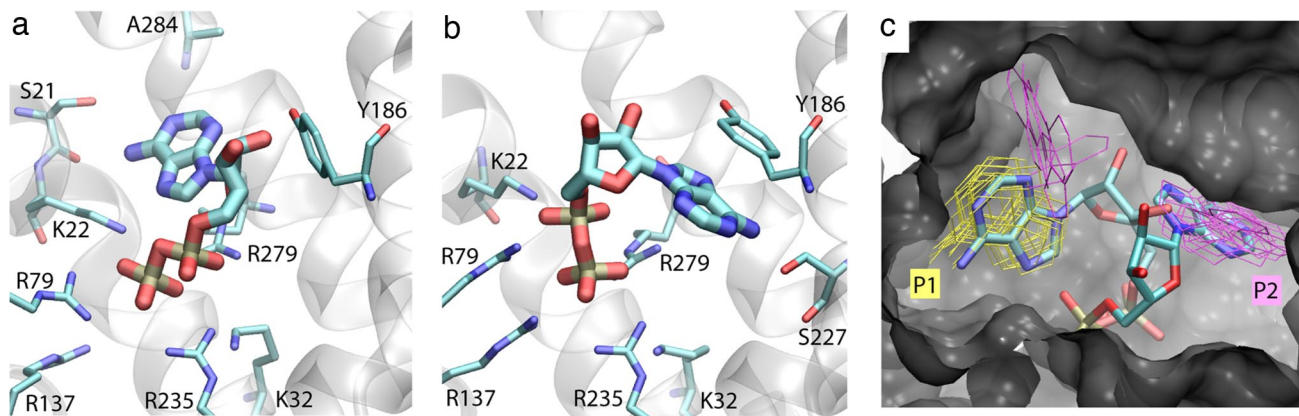


Fig. 4. ADP binding site. (a and b) ADP-binding pockets revealed by simulations NB4 (a) and NB2 (b) at $t = 100$ ns. The phosphate groups interact with K22, R79, and R279 as well as R235 from the bottom of the AAC vestibule. ADP also interacts with K32 via a water molecule in a and with R137 directly in b. (c) Superposition of simulations NB2 and NB4. ADP molecules at $t = 100$ ns are shown in stick representations. Snapshots of the adenine ring, taken at 5-ns intervals from the two simulations, are shown in purple (NB2) and yellow (NB4) lines. The two binding pockets of the adenine ring revealed by simulations NB4 and NB2 are labeled as P1 and P2, respectively.

-4 e, respectively), the positive potential of AAC can greatly improve the efficiency of substrate recruitment by the carrier. This is consistent with mutagenesis experiments revealing the importance of charged residues in the function of AAC (24–26). The positive potential of AAC may be of particular importance to ADP transport, because the inner mitochondrial membrane has a -0.18 to -0.2 -V transmembrane potential, disfavoring the transport of negatively charged species into the mitochondrial matrix.

The dynamics of Cl^- ions not only provides further evidence for the strong luminal electrostatic potential of AAC but also hints at additional roles for such a potential at the surface of the protein. In the absence of ADP (apo-AAC), Cl^- ions, which are initially placed in the bulk solvent to neutralize the simulation system, bind to the carrier within a few nanoseconds; at $t = 3$ ns, one Cl^- ion is found to enter the AAC vestibule, whereas two others adhered to the surface of AAC from the matrix side (Fig. S2). During the 55-ns-simulation, up to three Cl^- ions are found in the lumen simultaneously, the average number of luminal Cl^- being 1.9. However, these Cl^- ions do not show any specific binding and dynamically interact with multiple basic residues in the lumen. The two surface Cl^- ions, on the other hand, visit specific sites when they adhere to the surface of the protein. Interestingly, these sites are occupied by cardiolipin (negative) head groups in the crystal structure (8). The calculated electrostatic potential identifies these sites as strongly positive regions (Fig. S2c). This is in close agreement with the results of NMR experiments indicating that a large number of cardiolipins stay tightly bound to AAC even after isolation of the protein from the membrane (22, 23). Therefore, another role of the strong electrostatic potential in AAC might be in its insertion into the inner mitochondrial membrane that is rich in negative lipids [$\approx 20\%$ cardiolipins (9)]. The luminal electrostatic potential of AAC, which we find to be important for substrate recruitment, does not seem to be disrupted by the presence of negatively charged lipids *in vivo*; repeating the apo-AAC simulation with the three crystallographically solved cardiolipin molecules present in the lipid bilayer, we still measure a ≈ 1.2 -V electrostatic potential in the lumen and observe the entrance of a Cl^- ion into the vestibule in a 5-ns simulation (Table S1).

ADP-Binding Pockets. In an attempt to identify the ADP-bound state of AAC, we extended two of the binding simulations (NB2 and NB4) to $0.1 \mu\text{s}$ each (see animations in Movie S1 and Movie S2). These simulations revealed two binding modes for ADP, the

difference of which only concerns the position of the adenine ring, whereas the phosphate groups are found to occupy the same location. As shown in Fig. 4, ADP phosphate groups in both simulations form simultaneous, multiple salt bridges with the three basic residues (K22, R79, and R279) from region II (Fig. 3a) as well as R235 from region I at the bottom of the vestibule. The interactions between ADP and other residues from region I, either direct or water-mediated, are also observed, e.g., K32 in simulation NB4 and R137 in simulation NB2. In contrast to the single binding site identified for the phosphate groups, two major binding modes are found for the adenine ring. In simulation NB4, the base is accommodated by residues S21, K22, and A284 (pocket P1), whereas one of the hydroxyl groups of the sugar ring forms a hydrogen bond with Y186 (Fig. 4a). In simulation NB2, the adenine ring is buried deeply in a pocket (P2) formed by residue Y186, G182, I183, S227, and G224, where it maintains a stacking interaction with the phenyl ring of Y186 (Fig. 4b). A transient absence of the adenine ring from this pocket is observed in the middle of simulation NB2, during which the adenine ring visits a pocket formed by residues Q217, G280, T220, and A221 (Fig. 4c), whereas the phosphate groups remain in their binding site. The adenine ring stays at this position for ≈ 22 ns and then returns to pocket P2.

Most of the residues involved in the binding pockets, e.g., K22, R79, R279, Y186, and R235 are conserved among AACs of different species (8, 9). Moreover, the mutation of these residues has been shown to severely impair the transport activity (8, 24, 25). ADP in the binding pocket P2 is stabilized by a stacking interaction between its adenine ring and the aromatic residue Y186, which may render this location particularly favorable for nucleotide binding. The stacking interaction might also explain the selectivity of AAC against pyrimidine nucleotides, which have smaller base rings and therefore may not optimally interact with Y186 when their phosphate groups are engaged in salt-bridge interactions with the phosphate-binding site described above. In the binding pocket P2, the N6 group of ADP can form a hydrogen bond with the backbone oxygen of S227 (Fig. 4b). Because the N6 group is replaced by an oxygen in GDP, the loss of the hydrogen bond might contribute to the lower binding affinity of GDP and/or its inability to trigger conformational changes required for transport, which might form the basis for the selectivity of AAC for ADP over GDP.

The ADP-binding pocket P2 shows both similarities and differences compared with that suggested by a recent docking study (27, 28). The differences primarily concern the position of

odd-numbered helices in the apo-AAC are replaced by either “intrahelical” salt bridges or salt bridges between even-numbered and odd-numbered helices upon ADP binding (Fig. 5). This rearrangement “unlocks” the three odd-numbered helices, allowing the protein to expand in the matrix half.

Commonality of Electrostatic Features Among MCF Members. The distinct electrostatic features of AAC and their direct role in substrate binding and translocation prompted us to examine other members of the MCF family. The yeast *Saccharomyces cerevisiae* MCF family was chosen, because it includes the largest number of functionally characterized members (11). Among 34 yeast MCF members, 22 that are functionally characterized can be classified into three major groups according to their substrates (11): nucleotide carriers, amino acid transporters, and keto acid transporters. The substrates of four other MCF members have been suggested, including two transporters of CoA [Leu5p (31)] and FAD [Flx1p (32)] as well as two putative iron transporters [Mrs3p and Mrs4p (33, 34)]. We calculated total net charges for all 34 MCF members (Table S2), based on their primary structures obtained from the Saccharomyces Genome Database (www.yeastgenome.org). On average, a net charge of +15 e is found for 31 MCF members, whose substrates, if known, are either anionic or zwitterionic. The remaining three are the peroxisomal adenine nucleotide transporter Ant1p (−6 e), which is a nonmitochondrial MCF member, and two putative iron transporters Mrs3p (+4 e) and Mrs4p (+2 e), which have cationic substrates. Repeating the calculation for 1,067 yeast membrane proteins (the Yeast Membrane Protein Library, www.cbs.umn.edu/yeast/) results in an average charge of essentially zero (+0.3 e, see Fig. S4), indicating that a significantly large positive net charge is not an attribute shared by membrane proteins in general, but a distinct feature special to the MCF family.

Conclusions

The process of ligand binding is often difficult to capture in unbiased simulations because of the relatively short simulation time compared with the time scale on which the binding event occurs. To our knowledge, a complete ligand-binding event has not heretofore been described in full atomic detail by using unbiased simulations. The observed rapid, spontaneous binding of ADP to AAC demonstrates a strong attraction between the nucleotide and the protein, which is shown to result from an unusually strong (≈ 1.4 V) positive electrostatic potential of the lumen of the heavily charged AAC. Such a strong potential, which has not been observed in any other membrane proteins, funnels ADP molecules placed in different initial orientations into the same final orientation within a few nanoseconds. AAC can thus play an active role in recruiting nucleotide substrates, using its unique electrostatic features.

Our simulations have also identified putative ADP-binding sites, which are found to differ from the CATR-binding site revealed by the crystal structure. A notable difference between the two is the direct involvement of residues from the bottom of AAC vestibule in the binding of ADP. The observed deep penetration of ADP in our simulations results in a significant displacement of several basic residues, e.g., K22, R79, and R279, to deeper positions in the AAC lumen, where they begin to interfere with and disrupt the salt-bridge network at the bottom of the vestibule, thus initiating large-scale conformational transitions necessary for the nucleotide translocation.

By pulling a bound ADP molecule through the carrier, we have also probed the primary conformational changes of AAC during the ADP translocation. An outward motion of the three odd-numbered helices, which opens the matrix half of AAC, is revealed by these simulations. This process is initiated by the conversion of “interhelical” salt bridges connecting the odd-

numbered helices in the apo-AAC to either intrahelical salt bridges or salt bridges between even-numbered and odd-numbered helices. The rearrangement of salt bridges unlocks the three odd-numbered helices, allowing the protein to expand in the matrix half. As proposed by earlier experimental and theoretical studies (8, 27), proline residues from the MCF motif act as hinges during this process.

Finally, with a net charge calculation of yeast membrane proteins, we demonstrate that the mitochondrial carrier family exhibits distinct electrostatic features from other membrane proteins and that these features might play essential roles in distribution and function of these carriers. Because the inner mitochondrial membrane includes a significant fraction of negative lipids, the surface component of the positive charges carried by MCF members might enhance or even mediate partition of the protein into the mitochondrial membrane. More important, however, is the strong luminal component of the positive electrostatic potential, which exhibits a profound effect on the dynamics of substrate recruitment and translocation in AAC, an attribute that is very likely shared by other members of the MCF.

Methods

Modeling of AAC in Membrane. A 100×100 -Å² palmitoyl-oleoyl-phosphatidylcholine (POPC) bilayer was built by using the membrane plugin of the program VMD (35) with the membrane normal along the z axis. A 20-Å layer of water was added to each side of the bilayer. The hydrated membrane was first minimized for 5,000 steps and equilibrated for 500 ps at constant volume and temperature (NVT), with only the lipid tails free to move. This was then equilibrated for another 500 ps at constant pressure and temperature (NPT), with all atoms free to move. An AAC monomer [PDB ID 1okc (8)] was embedded in the equilibrated POPC bilayer. Missing residues (1 and 294–297) were added by using VMD (35). Water molecules resolved in the crystal structure were kept, whereas cardiolipin and CATR molecules were removed, except for the apo-AAC-CL simulation described below, where cardiolipin molecules were maintained. To embed AAC into the membrane, lipid molecules with heavy atoms closer than 0.8 Å to the protein were removed. To neutralize the charge of the protein, 19 Cl[−] ions were added, resulting in a final system of 80,955 atoms (Fig. 1a). A series of minimization and equilibration simulations were then performed to optimize the interaction between lipid tails and the protein: The system was first minimized for 5,000 steps and equilibrated under NVT condition for 200 ps, in which only the lipids were allowed to move. After 1,000 steps of minimization, another 200 ps of NPT equilibration was performed with the protein fixed. A last round of 1,000 steps of minimization was then performed, and the system was further equilibrated under NPT condition for 200 ps with the protein backbone constrained at 5 kcal/mol/Å².

Simulation Systems. For clarity, we will refer to the nucleotide-free AAC system described above as “apo-AAC.” After the minimization and equilibrations mentioned above, the apo-AAC system was further equilibrated for 55 ns under constant pressure in the z direction and constant temperature (NP_zT). The structure of the carrier remains close to the crystal structure during this simulation (root mean square deviation ≈ 2.0 Å), however, considerable fluctuation of the protein, especially in the IMS half, is evident, indicating the flexibility of the apo structure (Fig. S5). To examine the effect of cardiolipins on the electrostatic features of AAC, we have also built an apo-AAC-CL system in the same way as described above, with three cardiolipin molecules resolved in the crystal structure included in the lipid bilayer. This system was also simulated under NP_zT condition for 5 ns.

The ADP-AAC system was then built by adding ADP to the equilibrated apo-AAC system at $t = 1$ ns. ADP was added to the IMS side of the equilibrated apo-AAC in the bulk, ≈ 25 Å above the bottom of the basin and at least 5 Å away from any protein atoms (Fig. 1b). Three Cl[−] ions were removed to keep the system neutral. The phosphate groups of ADP were initially pointing toward the protein (Fig. 1b). This system was equilibrated for 10 ns under NP_zT condition and referred to as NB1, as listed in Table S1. To eliminate the effect of the initial orientation of ADP on the results, we built a second ADP-AAC system with the phosphate groups of ADP pointing away from the protein (Fig. 1c). Three independent simulations were performed to equilibrate this system under NP_zT condition: NB2, NB3, and NB4, which were 100, 15, and 100 ns long, respectively. An ATP-AAC system was then built in the same way as the ADP-AAC system in simulation NB1, except that ATP is placed 5 Å further away from AAC to ensure that no protein atoms are within 5 Å of the nucleotide. This system is equilibrated for 10 ns under NP_zT condition (Table S1).

To probe the initial conformational change of the matrix half of AAC, we then performed two independent nucleotide translocation simulations (NT1 and NT2) by means of steered MD (SMD) (36). These simulations were based on the ADP-binding simulation NB4 after its first 30 ns of equilibration. In these 20-ns-long simulations, the β -phosphorus atom of ADP was pulled along the $-z$ direction (toward the matrix side) by using a harmonic constraint moving at a velocity of 1.5 Å/ns and with a force constant (k) of 7.2 kcal/mol/Å². To prevent the overall translation of the system, the C α atoms of six peripheral protein residues (5, 97, 108, 202, 209, and 292) were harmonically constrained along the z direction ($k = 11.5$ kcal/mol/Å²).

Simulation Protocols. For all MD simulations, the program NAMD 2.6 (37) and the CHARMM27 parameter set with the CMAP correction (38, 39) were used. Langevin dynamics was used to keep the temperature constant at 310 K with a damping coefficient of 1 ps⁻¹. During pulling simulations, ADP was decoupled from the temperature bath. For NPT and NP_TT simulations, a Langevin piston (40) was used to maintain the pressure at 1 atm. Assuming periodic boundary conditions, the Particle Mesh Ewald (PME) method (41) with a grid density of at least 1/Å³ was used for computation of long-range electrostatic forces. All simulations were performed with time steps of 1, 2, and 4 fs for bonded, nonbonded, and PME calculation, respectively.

Electrostatic Calculations. The electrostatic potential of the apo-AAC system is calculated by using the PMEPOD plugin of VMD (42), with a grid spacing of <1

Å. Because Cl⁻ ions become bound with the protein after ≈ 2 -ns simulation, we calculated the electrostatic potential for the apo-AAC system using the first 2 ns of simulation. The resulting potential is an average over the periods of simulations mentioned above. Assuming a generic titration state for side chains, i.e., glutamates and aspartates negative and lysines and arginines positive, net charges of the yeast MCF members were calculated based on their sequences from the Saccharomyces Genome Database (www.yeastgenome.org/). To examine whether mitochondrial carriers show distinct charge characteristics from other yeast membrane proteins, we repeated the calculation for every protein in the Yeast Membrane Protein Library (www.cbs.umn.edu/yeast/). Among 1,593 sequences in the library, 1,067 sequences with a minimum of 200 aa were selected for the comparative analysis (MCF members are ≈ 300 aa long). Normalizing the net charge of each protein by its amino acid count, we then obtained the net charge density of the 1,067 yeast membrane proteins. A histogram representing the net charge density distribution of these proteins was then built by using a bin width of 0.003 e/aa (Fig. S4).

ACKNOWLEDGMENTS. We acknowledge computer time provided by the Large Resource Allocation Committee (MCA06N060), specially on the BigRed cluster at Indiana University, Bloomington, IN, and computer time on the National Center for Supercomputing Applications Abe Cluster and the Turing Xserve Cluster at the University of Illinois at Urbana-Champaign. This work was supported by National Institutes of Health Grant R01-GM067887.

- Duee ED, Vignais P (1965) Exchange between extra- and intramitochondrial adenine nucleotides. *Biochim Biophys Acta* 107:184–188.
- Pfaff E, Klingenberg M, Heldt HW (1965) Unspecific permeation and specific exchange of adenine nucleotides in liver mitochondria. *Biochim Biophys Acta* 104:312–315.
- Klingenberg M (1977) The adenine-nucleotide exchange in submitochondrial (sonic) particles. *Eur J Biochem* 76:553–565.
- Klingenberg M (1980) The ADP-ATP translocation in mitochondria, a membrane potential controlled transport. *J Membr Biol* 56:97–105.
- Aquila H, Misra D, Eulitz M, Klingenberg M (1982) Complete amino acid sequence of the ADP/ATP carrier from beef heart mitochondria. *Hoppe Seylers Z Physiol Chem* 363:345–349.
- Klingenberg M (1985) The ADP/ATP carrier in mitochondrial membranes. *The Enzymes of Biological Membranes*, ed, Martonosi A (Plenum, New York), pp 511–553.
- Klingenberg M (1989) Molecular aspects of the adenine nucleotide carrier from mitochondria. *Arch Biochem Biophys* 270:1–14.
- Pebay-Peyroula E, et al. (2003) Structure of mitochondrial ADP/ATP carrier in complex with carboxyatractyloside. *Nature* 426:39–44.
- Nury H, et al. (2006) Relations between structure and function of the mitochondrial ADP/ATP carrier. *Annu Rev Biochem* 75:713–741.
- Walker JE (1992) The mitochondrial transporter family. *Curr Opin Struct Biol* 2:519–526.
- Kunji ER (2004) The role and structure of mitochondrial carriers. *FEBS Lett* 564:239–244.
- Aquila H, Link TA, Klingenberg M (1987) Solute carriers involved in energy transfer of mitochondria form a homologous protein family. *FEBS Lett* 212:1–9.
- Brandolin G, Boulay F, Dalbon P, Vignais PV (1989) Orientation of the N-terminal region of the membrane-bound ADP/ATP carrier protein explored by antipeptide antibodies and an arginine-specific endoprotease. Evidence that the accessibility of the N-terminal residues depends on the conformational state of the carrier. *Biochemistry* 28:1093–1100.
- Trézéguet V, et al. (2000) A covalent tandem dimer of the mitochondrial ADP/ATP carrier is functional *in vivo*. *Biochim Biophys Acta* 1457:81–93.
- Tajkhorshid E, et al. (2002) Control of the selectivity of the aquaporin water channel family by global orientational tuning. *Science* 296:525–530.
- Wang Y, Schulten K, Tajkhorshid E (2005) What makes an aquaporin a glycerol channel: A comparative study of AqpZ and GlpF. *Structure (London)* 13:1107–1118.
- Gumbart J, Wang Y, Aksimentiev A, Tajkhorshid E, Schulten K (2005) Molecular dynamics simulations of proteins in lipid bilayers. *Curr Opin Struct Biol* 15:423–431.
- Gumbart J, Wiener MC, Tajkhorshid E (2007) Mechanics of force propagation in TonB-dependent outer membrane transport. *Biophys J* 93:496–504.
- Falconi M, et al. (2006) Structural dynamics of the mitochondrial ADP/ATP carrier revealed by molecular dynamics simulation studies. *Proteins* 65:681–691.
- Törnroth-Horsefield S, et al. (2006) Structural mechanism of plant aquaporin gating. *Nature* 439:688–694.
- Fan H, Mark AE, Zhu J, Honig B (2005) Comparative study of generalized born models: Protein dynamics. *Proc Natl Acad Sci USA* 102:6760–6764.
- Beyer K, Klingenberg M (1985) ADP/ATP carrier protein from beef heart mitochondria has high amounts of tightly bound cardiolipin, as revealed by phosphorus-31 nuclear magnetic resonance. *Biochemistry* 24:3821–3826.
- Brustovetsky N, Klingenberg M (1996) Mitochondrial ADP/ATP carrier can be reversibly converted into a large channel by Ca²⁺. *Biochemistry* 35:8483–8488.
- Müller V, Basset G, Nelson DR, Klingenberg M (1996) Probing the role of positive residues in the ADP/ATP carrier from yeast. The effect of six arginine mutations on oxidative phosphorylation and AAC expression. *Biochemistry* 35:16132–16143.
- Müller V, Heidkämper D, Nelson DR, Klingenberg M (1997) Mutagenesis of some positive and negative residues occurring in repeat triad residues in the ADP/ATP carrier from yeast. *Biochemistry* 36:16008–16018.
- Nelson DR, Felix CM, Swanson JM (1998) Highly conserved charge-pair networks in the mitochondrial carrier family. *J Mol Biol* 277:285–308.
- Kunji ER, Robinson AJ (2006) The conserved substrate binding site of mitochondrial carriers. *Biochim Biophys Acta* 1757:1237–1248.
- Robinson AJ, Kunji ER (2006) Mitochondrial carriers in the cytoplasmic state have a common substrate binding site. *Proc Natl Acad Sci USA* 103:2617–2622.
- Klingenberg M (2007) Transport viewed as a catalytic process. *Biochimie* 89:1042–1048.
- Klingenberg M (1991) Mechanistic and energetic aspects of carrier catalysis—exemplified with mitochondrial translocators. *A Study of Enzymes*, ed, Kuby S (CRC, Boca Raton, FL), Vol II, pp 367–388.
- Prohl C, et al. (2001) The yeast mitochondrial carrier leu5p and its human homologue Graves' disease protein are required for accumulation of coenzyme a in the matrix. *Mol Cell Biol* 21:1089–1097.
- Tzagoloff A, Jang J, Jerum DM, Wu M (1996) Flx1 codes for a carrier protein involved in maintaining a proper balance of flavin nucleotides in yeast mitochondria. *J Biol Chem* 271:7392–7397.
- Mühlenhoff U, et al. (2003) A specific role of the yeast mitochondrial carriers mrs3/4p in mitochondrial iron acquisition under iron-limiting conditions. *J Biol Chem* 278:40612–40620.
- Zhang Y, Lyver ER, Knight SA, Lesuisse E, Dancis A (2005) Frataxin and mitochondrial carrier proteins, mrs3p and mrs4p, cooperate in providing iron for heme synthesis. *J Biol Chem* 280:19794–19807.
- Humphrey W, Dalke A, Schulten K (1996) VMD—Visual Molecular Dynamics. *J Mol Graphics* 14:33–38.
- Sotomayor M, Schulten K (2007) Single-molecule experiments *in vitro* and *in silico*. *Science* 316:1144–1148.
- Phillips JC, et al. (2005) Scalable molecular dynamics with NAMD. *J Comp Chem* 26:1781–1802.
- Schlenkerich M, Brickmann J, MacKerell A D, Jr, Karplus M (1996) Empirical potential energy function for phospholipids: Criteria for parameter optimization and applications. *Biological Membranes: A Molecular Perspective from Computation and Experiment*, eds, Merz K M, Roux B (Birkhauser, Boston), pp 31–81.
- MacKerell A, Jr., et al. (1998) All-atom empirical potential for molecular modeling and dynamics studies of proteins. *J Phys Chem B* 102:3586–3616.
- Feller SE, Zhang YH, Pastor RW, Brooks BR (1995) Constant pressure molecular dynamics simulation—the Langevin piston method. *J Chem Phys* 103:4613–4621.
- Darden T, York D, Pedersen L (1993) Particle mesh Ewald. An N-log(N) method for Ewald sums in large systems. *J Chem Phys* 98:10089–10092.
- Aksimentiev A, Schulten K (2005) Imaging alpha-hemolysin with molecular dynamics: Ionic conductance, osmotic permeability and the electrostatic potential map. *Biophys J* 88:3745–3761.